Tuning electron transfer by crystal facet engineering of $BiVO_4$ for boosting visible-light driven photocatalytic reduction of bromate

Liu, Guoshuai; Zhu, Yukun; Yan, Qun; Wang, Han; Wu, Peng; Shen, Yaoliang; Doekhi-Bennani, Yasmina

DOI
10.1016/j.scitotenv.2020.143086

Publication date
2021

Document Version
Accepted author manuscript

Published in
Science of the Total Environment

Manuscript for: *Science of the Total Environment*
Submission date: 12-10-2020

Tuning Electron Transfer by Crystal Facet Engineering of $BiVO_4$ for Boosting Visible-Light Driven Photocatalytic Reduction of Bromate

Guoshuai Liu[a‡], Yukun Zhu[b‡], Qun Yan[a,c,*], Han Wang[a], Peng Wu[c], Yaoliang Shen[c], and Yasmina Doekhi-Bennani[d]

[a] *School of Environmental and Civil Engineering, Jiangnan University, Wuxi 214122, China*

[b] *School of Environmental Science and Engineering, State Key Laboratory of Bio-fibers and Eco-textiles, Qingdao University, Qingdao 266071, China*

[c] *Jiangsu Collaborative Innovation Center of Technology and Material of Water Treatment, Suzhou 215011, China*

[d] *Department of Water Management, Section Sanitary Engineering, Delft University of Technology, PO Box 5048, 2600 GA Delft, The Netherlands*

[‡] *The authors contribute equally to this work.*

Corresponding author:

* Qun Yan

School of Environmental and Civil Engineering, Jiangnan University, Wuxi 214122, China.

E–mail: yanqun@jiangnan.edu.cn (Q. Yan).

ABSTRACT:

Removal of bromate (BrO_3^-) has gained increasing attention in drinking water treatment process. Photocatalysis technology is an effective strategy for bromate removal. During the photocatalytic reduction of bromate process, the photo-generated electrons are reductive species toward bromate reduction and photo-generated holes responsible for water oxidation. In this study, the monoclinic bismuth vanadate ($BiVO_4$) single crystal was developed as a visible photocatalyst for the effective removal of bromate. The as-synthesized $BiVO_4$ photocatalyst with optimized {010} and {110} facets ratio could achieve almost 100% removal efficiency of BrO_3^- driven by visible light with a first-order kinetic constant of 0.0368 min^{-1}. As demonstrated by the electron scavenger experiment and density functional theory (DFT) calculations, the exposed facets of $BiVO_4$ should account for the high photocatalytic reduction efficiency. Under visible light illumination, the photo-generated electron and holes were spatially transferred to {010} facets and {110} facets, respectively. The $BiVO_4$ single crystal photocatalyst may serve as an attractive photocatalyst by virtue of its response to the visible light, spatially charge transfer and separation as well as high photocatalytic activity, which will make the removal of BrO_3^- in water much easier, more economical and more sustainable.

Keywords: bromate; bismuth vanadate; photocatalysis; crystal engineering

INTRODUCTION

Bromate (BrO_3^-) originated from the chlorination or ozonation process in bromide-containing water has attracted the attention of many researchers (Bouland et al., 2005; Chen et al., 2016; Parker et al., 2014, Zhu et al.,). The drinking water standard of BrO_3^- in the European Union and the U.S. Environmental Protection Agency is less than 10 μg/L (Shen et al., 2017; Weinberg et al., 2003; Wu et al., 2013). To overcome this obstacle, considerable progress has been made regarding the transformation of BrO_3^- to Br^- by using various technologies, such as electrochemical reductive treatment (Xie and Shang, 2007), zero-valent iron (Wang et al., 2009; Zhang et al., 2015) and FeOOH catalytic reduction (Nie et al., 2014). Although these already established technologies can remove BrO_3^- effectively, they may suffer from various problems such as high cost, operational complexity, as well as the potential secondary pollution risk induced by metal leaching (Ayoubi-Feiz et al., 2015; Lin et al., 2016; Noguchi et al., 2003).

Recently, photocatalysis process was regarded as a superior technology to remove BrO_3^- (Noguchi et al., 2002). Compared with the conventional removal methods mentioned above, photocatalysis shows fascinating potential for bromate removal systems due to its high efficiency, low-cost and environmental benignity (Ayoubi-Feiz et al., 2015; Lin et al., 2016; Noguchi et al., 2003). As the widely used photocatalyst, TiO_2 based photocatalysts had been extensively employed in bromate removal by UV-light driven photocatalysis, whereas the efficient conversion of BrO_3^- to Br^- was contributed to the photo-generated electrons at conduction band (CB) (Li et al., 2016; Liu et al., 2016; Zhang et al., 2005).

However, the photocatalytic systems based on TiO_2-photocatalysis still suffer from some problems for bromate removal: (i) The wide bandgap (E_g = 3.2 eV) of TiO_2 can only be responsively under UV light irradiation (UV, 3% ratio of solar light). This may cause inconvenience in practical applications (Perry et al., 2009; Williams et al., 2008; Yang et al., 2020a; Yang et al., 2020b). (ii) The reducing agent in the photocatalytic system is photo-generated electrons. It is important to improve the

77 quantum efficiency of photoelectrons to participate in the bromate reduction reaction (Pan and Zhu,
78 2010; Wang et al., 2020a; Yang et al., 2019; Zhu et al., 2020c; Wang et al., 2020b; Wang et al., 2019).
79 (iii) As a redox couple in the reaction depends on generated-electrons and holes, the photocatalytic
80 reduction half-reaction is interdependent to the oxidation half-reaction mediated by photo-generated
81 holes at the valence band (VB). Therefore, there is a growing interest in developing high overall
82 efficiency visible light driving photocatalysts (Zhang et al., 2019; Zhu et al., 2019; Zhu et al.,
83 2020a).

84 In the BrO_3^- reduction system, BrO_3^- acts as an electron acceptor, and the reduction reaction (1 e^-
85 process) is not considered as a limiting step for the overall photocatalytic redox reaction. On the
86 other hand, the oxidation of water (4 e^- process) is observed as a bottleneck or the rate-determining
87 step (Zhu et al., 2020b). Based on the above-mentioned points, the premise for effective BrO_3^-
88 reduction is to find a visible photocatalyst with high reductive activity, high selectivity and water
89 oxidation ability.

90 Monoclinic $BiVO_4$ has been widely used in photocatalysis or photoelectrochemical process for the
91 water oxidation to produce oxygen due to its efficient and active visible light photocatalytic
92 properties (Nakabayashi et al., 2017; Saison et al., 2015). Therefore, the oxidation reaction would not
93 hamper the reductive half-reaction (bromate reduction reaction). On the premise that $BiVO_4$ can
94 efficiently oxidize water, the major water oxidation products are oxygen rather than hydroxyl
95 radicals (Nakabayashi et al., 2017; Saison et al., 2015). This can mitigate the problem of the
96 re-oxidation of bromine ions by hydroxyl radicals. Recent associated studies on the preparation of
97 single crystal $BiVO_4$ photocatalysts have shown that photo-generated carriers could be transferred to
98 different exposed crystal facets (Li et al., 2013; Zhu et al., 2017), the reduction and oxidation
99 reactions were spatially separated with a high reaction extent. Learned from these experiences, the
100 reduction surface (photo-generated electron rich surface) of $BiVO_4$ can be made by the crystal facet
101 engineering, thus improving the quantum efficiency of photo-generated electrons involved in the

bromate reduction reaction.

Herein, three kinds of $BiVO_4$ crystals (BVO-a, b and c) with different exposed facets were prepared and applied to the photocatalytic reduction of bromate under visible light. Additionally, the structure and morphology of $BiVO_4$ single crystals were characterized using X-ray diffraction (XRD) and field emission scanning electron microscopy (FESEM). Furthermore, the BrO_3^- reduction performance was evaluated by calculating the conversion of BrO_3^- to Br^-. Lastly, the optical properties and electron configuration were estimated using density functional theory (DFT), and the bandgap, band position, and effective electron mass were also taken into consideration. The possible photocatalytic reduction mechanisms of BrO_3^- by $BiVO_4$ crystals were proposed.

EXPERIMENTAL SECTION

Synthesis of the photocatalyst. $BiVO_4$ powders were prepared by liquid-solid state reaction. 5 mmol of V_2O_5 and 10 mmol of $Bi(NO_3)_3{\cdot}5H_2O$ were added in 60 mL of DI water. The precursor solution was stirred until a yellow solution was formed. The pH of the solution was regulated to 1.0, 0.5 and 0.1 by ammonia solution or dilute nitric acid solution, and then the solution was vigorously stirred at room temperature for 5 days. The obtained $BiVO_4$ powder was separated by centrifugation, washed with DI water and dried at 60 °C. Moreover, the obtained $BiVO_4$ powders synthesized at different pH values of 1.0, 0.5 and 0.1 were labeled as $BiVO_4$-a, $BiVO_4$-b and $BiVO_4$-c.

Characterization. The powder X-ray diffraction (XRD) characterization was conducted on an X-ray diffractometer (Bruker D8 Adv., Germany). The crystalline phase and morphology of the as-prepared $BiVO_4$ samples were characterized by an X-ray diffractometer (Bruker D8 Adv., Germany) and afield emission scanning electron microscope (FESEM, Type-4800, Hitachi, Japan), respectively. A spectrophotometer (Type-UV2550, Shimadzu, Japan) recorded the UV−vis diffuse reflectance spectroscopy (DRS) of the powders. The photoelectrochemical measurements were conducted using a CHI760E electrochemical workstation. The photocurrent measurements were carried out under visible light irradiation (300 W Xenon lamp).

Theoretical Calculations. The optimization of the unit cell of monoclinic scheelite $BiVO_4$ was performed using the CASTEP code with the projector augmented wave (PAW) pseudopotentials (Liu et al., 2017), and the parameter was set according to the reference (Long et al., 2008). The angle b of monoclinic scheelite $BiVO_4$ was set to 134.9° for simplification, the detailed parameters can be found in Table S1. The stable crystal configuration of the bulk and the cleavage surface with the optimized lowest energy are shown in Figure S1.

Experimental Setup and Procedures. The BrO_3^- ions removal performance was tested according to the previous method reported by our team (Liu et al., 2019). Both BrO_3^- and Br^- ions were determined by an ion chromatograph analyzer (LC-10A, Shimadzu, Japan).

RESULTS AND DISCUSSION

Characterization of $BiVO_4$ Photocatalysts. The XRD patterns of three types of as-synthesized $BiVO_4$ photocatalysts are presented in Figure 1A. All diffraction patterns of samples ($BiVO_4$-a, b and c) showed sharp diffraction peaks and all typical peaks were attributed to monoclinic scheelite $BiVO_4$ crystal phase (JCPDS No. 14-0688, space group: *C*2/*c*), evidently suggesting that the $BiVO_4$ photocatalysts have high crystallinity (Liu et al., 2014). Considering the phenomenon that the (121) peak was the highest peak for separated $BiVO_4$-a, b and c, the (121) peak was selected as the benchmark to evaluate the possible exposed surface in $BiVO_4$ crystal qualitatively, i.e., the intensity ratios of the diffraction peak of (040) and (110) compared with (121). The intensityof (040) diffraction peak followed the order of $BiVO_4$-a > $BiVO_4$-b > $BiVO_4$-c, while that of (110) diffraction peak showed a reverse order, i.e., $BiVO_4$-c > $BiVO_4$-b > $BiVO_4$-a. However, the intensity of (110) diffraction peak of $BiVO_4$-c was stronger than that of $BiVO_4$-b and a ($BiVO_4$-c > $BiVO_4$-b > $BiVO_4$-a). According to Wang's study, this intensity difference in XRD pattern indicated that the (040) diffraction peak was the dominant peak for $BiVO_4$-a, and that for $BiVO_4$-c was (110) (Wang et al., 2011). The FESEM image of $BiVO_4$-a exhibited a sheet-like geometry with a length of 1.5 μm, width of 400-nm, and thickness of 150-nm, respectively (Figure 1B). The $BiVO_4$-b sample exhibited

a polyhedral box shape (Figure 1C) with an average size of about 1.5 μm. In addition, the $BiVO_4$-c with an octahedral shape of about 2 μ m was observed in Figure1D. To further identify the exposed crystal faces, the corresponding HRTEM image for $BiVO_4$-a is given in Figure 1E.

The corresponding selected area electron diffraction (SAED) pattern in Figure 1F (inset picture) is taken from the sheet-like $BiVO_4$-a sample (Figure 1E), revealing the growth orientation in accordance with the results of XRD measurements. As determined by XRD result, and with different b axis orientations for different sheets, the d spacings measured from SAED (zone axis [010]) were 2.61 Å, which agreed well with the lattice spacings of (200) monoclinic $BiVO_4$ (Wang et al., 2011). The growth direction was along the (040) facet, i.e., {010} crystal planes; therefore, the sheet-like $BiVO_4$-a growed along the b axis as seen in the HRTEM images (Figure 1F). Based on these analyses and calculations, a simple schematic illustration of the exposed crystal surface is presented in the insets in Figure 1B, C and D according to the XRD and HRTEM analysis. The XPS spectra of Bi 4f, V 2p and O 1s are illustrated in Figure S2. The Bi 4f consisted of two peaks at the binding energy of 156.3 and 161.5 eV, while the V 2p spectra showed two peaks of 514.0 eV and 521.7 eV, respectively. Moreover, the O 1s spectra was detected at the binding energy of 527.1 eV.

Figure 1 (A-F)

Photocatalytic Reduction of BrO_3^- by $BiVO_4$ Photocatalysts. The feasibility of photocatalytic reduction of BrO_3^- using $BiVO_4$ photocatalysts under visible light irradiation irradiation were examined by photocatalytic experiment. No BrO_3^- reduction was observed in the absence of photocatalysts, which excluded the direct visible light driven photolysis of BrO_3^- reduction. As illustrated in Figure 2A, the concentration of BrO_3^- decreased from initial 1000 to 0 μg L^{-1} (below the detection limit) for $BiVO_4$-b after 150 minutes of reaction, which exhibited almost 100% BrO_3^- removal efficiency. However, $BiVO_4$-a and $BiVO_4$-c reduced the initial BrO_3^- concentration (1000

177 μg L^{-1}) to 130 and 230 μg L^{-1}, respectively. The BrO_3^- removal performance can be well indexed to
178 the first-order reaction k = 0.0368 min^{-1} for $BiVO_4$-b (Figure 2B), which was 2.08 and 3.94 times
179 higher than that of $BiVO_4$-a (0.0177 min^{-1}) and $BiVO_4$-c (0.0094 min^{-1}), respectively. (Table S2).
180 These results demonstrated that the $BiVO_4$-b sample showed superior photocatalytic bromate
181 removal performance than that of $BiVO_4$-a and -c samples which might be benefited from the facet
182 effect of $BiVO_4$ crystal. Moreover, the stability of the $BiVO_4$ photocatalysts was also evaluated and
183 the result can be seen in Figure S3. during the recycling process, the photocatalytic performance of
184 $BiVO_4$ was with high stability, amount to 3% activity loss after five-cycles. During the recycling
185 process, the photocatalytic performance of $BiVO_4$ was of high stability with the activity loss
186 amounting to 3% activity loss after five-cycles
187
188 **Figure 2 (A and B)**
189
190 **Mechanisms Insight.** To further understand the BrO_3^- reduction mechanism by $BiVO_4$
191 photocatalyst, the electron scavenger experiments were implemented by adding $S_2O_8^{2-}$ (Romão et al.,
192 2015). As a typical electron scavenger, the degradation performance of BrO_3^- was decreased
193 obviously after the introduction of $S_2O_8^{2-}$ (Figure S4 and Table S3). Notably, the bromate removal
194 nearly disappeared when 5 mmol of $K_2S_2O_8$ was added. Thus, it could be concluded that the
195 photo-generated electrons were the reactive species during the BrO_3^- photocatalytic reduction
196 process.
197 As we know, for semiconductor photocatalysis, the optical properties are directly related to the
198 intrinsic electron configuration and thus influence the photocatalytic performance. Figure 3A shows
199 the DRS spectra of $BiVO_4$ samples with different exposed surfaces. The adsorption properties of the
200 obtained three types of $BiVO_4$ were all typical visible light-driven photocatalysts with an absorption
201 edge at approximately 536 nm (E_g = 2.31 eV), which was in line with the previous report (Su et al.,

2011). The DFT calculation regarding optical properties was conducted to better understand the relationship of light absorption with exposed surface. As shown in Figure 3B, there was no obvious difference in the absorption threshold for polycrystal, {010} and {110} facets $BiVO_4$, respectively, which was in accordance with the DRS results. Based on the above DRS and DFT calculation results, it can be concluded that the optical properties of $BiVO_4$ samples may not be the major reasons for the great difference in the photocatalytic removal of bromate.

Figure 3 (A and B)

$$E_{VB} = \chi - E^e + \frac{E_g}{2} \quad (1)$$

$$E_{CB} = E_{VB} - E_g \quad (2)$$

Furthermore, the theoretical positions of energy band position of $BiVO_4$ at pH = pH_{pzc} were calculated using the following conventional eqn. 1 and 2 (Xu and Schoonen, 2000). E_e is the free electron energy (4.5 V), E_g is the measured band gap. By substituting these absolute electronegativities of Bi, V and O to eqn. 1 and 2, the E_{VB} of 2.80 V and E_{CB} of 0.49 V (SHE) were obtained (Cooper et al., 2014). Although the valence band position of $BiVO_4$ was suitable for hydroxyl radicals generation, according to the previous literature, $BiVO_4$ was generally considered as a highly efficient photocatalyst for water oxidation to produce oxygen rather than hydroxyl radicals, thus making the reduction of BrO_3^- more efficient towards Br^- conversion (Nakabayashi et al., 2017; Saison et al., 2015).

As shown in Figure S1, VO_4^{3-} was a stretched tetrahedron. In the stretched BiO_8 dodecahedron, Bi atoms were surrounded by 8 O atoms, and the four bond lengths were different (2.467, 2.466, 2.471, and 2.528 Å) (Stoltzfus et al., 2007; Yang et al., 2013). As we know, the dipole moments played an important role in photocatalysis, especially on the effective separation of carriers. A big dipole

moment always means a high driving force makes efficient photo-generated carriers transfer (Li et al., 2014). In this regard, the absolute numerical value of dipole moment is calculated to be 0.79 and 0.68 D on {010} and {110} facets, respectively. The larger dipole moment of the BiO polyhedrons for {010} facet demonstrates greater distortion of the {110} surface layer, hence leading to a larger internal polarization which is conducive to the charge separation and higher activity for the photocatalytic reduction of BrO_3^-.

Table 1

To further understand the electronic configuration of the two exposed crystal facets, the band structure of $BiVO_4$ is plotted in Figure 4A. Considering the symmetry of the monoclinic system, the path selected from the Brillouin zone was along Z → G→ Y → A → B → D → E → C. The DFT calculated E_g for $BiVO_4$ was 2.12 eV, close to the experimental value (2.31 eV). The highest band energy level and lowest energy level were located at different K-points, which indicated the typical indirect band gap property. Furthermore, we can calculate the effective carrier masses of {010} and {110} facets based on the curvatures of the bands in the corresponding directions by fitting parabolic functions to the conduction band minimum (CBM) and valence band maximum (VBM) of $BiVO_4$. According to the Eq. (3) (Li et al., 2014), the effective electron masses can be estimated, where k is the wave vector, and E_k is the energy corresponding to the wave vector k.

$$m^* = \pm h^2 \left(\frac{d^2 E_k}{dk^2}\right)^{-1} \quad (3)$$

The calculated results are summarized in Table 1.The effective electron masses were approximately 0.13 m_0 and 0.30 m_0, and the effective hole masses are estimated to be approximately 0.18 m_0 and 0.57 m_0 for {010} and {110} surfaces, respectively. In the photocatalytic process, lower effective mass means higher drift velocity, and the photo-generated hole/electron pairs could be transfered to the surface of photocatalyst (Li et al., 2014). Therefore, the effective electron mass of {010} was

0.13 m_0, obviously lower than that of {110} facets making it favorable for the photocatalytic bromate reduction process.

Figure 4 (A and B)

According to the dipole moment and charge transport calculation, the presence of {010} facet exposed $BiVO_4$ was beneficial for the charge separation. As revealed from the photocurrent of $BiVO_4$-a, $BiVO_4$-b and $BiVO_4$-c in Figure 4B, $BiVO_4$-b possessed a much higher photocurrent than $BiVO_4$-a and $BiVO_4$-c. The intense photocurrent generally means a higher hole/electron pairs separation efficiency (Li et al.). As shown in Figure 4B, the $BiVO_4$-b sample with {010} facet exposed maintained a high separation efficiency of hole/electron pairs, which was in well agreement with the result of dipole moment calculations.

The intrinsic reason for the separation of photo-generated carriers on the {010} and {110} of $BiVO_4$ crystal facets was evaluated by the DFT calculation method (Pan et al., 2011). Figure 5A shows the density of states (DOS) calculation results (where Fermi energy was set as 0 eV).We can ascertain the conduction band edge and valence band edge from Figure 5A, where the conduction band edge for {110} facets was 1.33 eV, and that for {010} was 2.15 eV. Thus, the energy differences for conduction bands (Δ_{CB}) between {010} and {110} facets was about 0.82 eV. Similarly, we could calculate the Δ_{VB} by analyzing the DOS curves and the result is about 0.20 eV between {010} and {110} facets. The existed difference well demonstrated that the transfer trend of photo-generated electron was from {110} to {010} facets in the thermodynamic view. Within this context, the electrons were accumulated on {010} facets, whereas the holes were enriched on {110} facets. Based on the calculated results obtained in Figure 5A, the schematic diagram of spatial photo-generated carriers separation between {110} and {010} facets is schematic shown in Figure 5B. Furthermore, the Work function (W) calculation results are shown in Figure 5C and 5D. The W of {010} and {110}

facets was 6.2 eV and 4.5 eV, respectively. The W value of {010} facets is obvious bigger than that of {110} facets, which makes the {010} facets have a higher electron capture ability (Gao et al., 2011). The results were in line with the density of state (DOS) analysis, where the photo-generated electrons were separated spatially with the photo-generated holes during photocatalytic process to form electron-rich {010} facets and hole-rich {110} facets.

Figure 5 (A, B, C and D)

For a practical photocatalytic reaction, reduction reactions were accompanied by oxidation reactions. To achieve a high photocatalytic efficiency (in this study, is photocatalytic reduction of bromate), high oxidation reactions involved by photo-generated holes must be considered. To clarify the mechanism deeply, the test of $BiVO_4$ photocatalyst utilized in water oxidation under visible light irradiation of O_2 evolution with BrO_3^- as electron sacrificial agent ($NaBrO_3$, 0.1 mol L^{-1}) was conducted, and the photocatalytic O_2 evolution performance is shown in Table S4. As shown in Table S4, the $BiVO_4$-b exhibited the highest oxygen production with the rate of 11.70 μmol h^{-1}, and the order of oxygen production rate was $BiVO_4$-b (11.70 μmol h^{-1}) >> $BiVO_4$-a (2.30 μmol h^{-1}) > $BiVO_4$-c (1.50 μmol h^{-1}). The results evidently confirmed that the $BiVO_4$-b showed the highest water oxidation, as an overall reaction, the photo-reduction performance was correlated with the oxidation ability. Therefore, the $BiVO_4$-b sample with an optimized exposure ratio of the {010} and {110} surfaces exhibited the highest photocatalytic bromate reduction activity. The conceivable intrinsic mechanisms are schematically showed in Figure 6. Under the irradiation of visible light, photo-generated carriers were separated toward different surfaces for the polyhedral box shape $BiVO_4$ photocatalyst, i.e., the photo-generated electrons (thermodynamic potential of 0.49 V, SHE) and photo-generated holes (2.80 V, SHE) were transferred to different facets of $BiVO_4$ crystal. As shown in Figure 6, the {010} facets were the electron-rich surfaces, whereas the holes were

accumulated on the {110} surfaces. The electron with a redox potential of 0.49 V was a robust reductive for bromate reduction (BrO_3^- + $6H^+$ + $6e^-$ → Br^- + $3H_2O$, $E^\ominus$ = 1.423 V). And photo-generated hole with a high redox potential of 2.80 V could decompose H_2O to produce oxygen efficiently ($2H_2O - 4e^- \rightarrow O_2 + 4H^+$, $E^\ominus$ = 1.23 V). In this manner, BrO_3^- could be regarded as the electron acceptor and *in-situ* reduced at {010} facets, while the water oxidation reaction was occurred at {110} surfaces to produce O_2. The photo-generated electron-hole pairs were spatially separated, and the oxidation and reduction reactions occurred at different crystal facets; thus, a high bromate reduction efficiency and selectivity on $BiVO_4$ single crystal with optimized {010} and {110} ratio could be achieved. Besides, a systemic comparison with conventional photocatalyst of TiO_2, traditional bulk $BiVO_4$ or Bi_2MoO_6 documented from literatureis summarized in Table S5. The $BiVO_4$-b sample with active exposed facets ratio could remove almost 100% of BrO_3^-, whose kinetic constant was significantly higher than that of other conventional photocatalysts.

Figure 6

Conclusions. To achieve efficient removal of BrO_3^-, we herein developed single crystal photocatalysts $BiVO_4$ with different exposed facets. The {010} facets are exposed electron-rich surfaces with a higher dipole moment and a lower effective masse of electrons/holes, which is more favorable for the photocatalytic bromate reduction reaction. Under visible light illumination, the photo-generated reductive electrons and oxidative photo-generated holes are spatially transported to {010} and {110} facets, respectively. During the bromate photocatalytic removal process, water acts as an electron donor, thus avoiding the risk of secondary pollution, making the BrO_3^- removal of high efficiency. This investigation provides a simple and effective strategy for enhanced degradation of bromate without complicated preparation procedure, which makes the bromate removal more efficient and sustainable, and also gives a guideline for the development of single crystal

photocatalyst for bromate photocatalytic reduction.

ACKNOWLEDGEMENTS

National Key Research and Development Program of China (2017YFE9133400), Pre-research Fund of Jiangsu Collaborative Innovation Center of Technology and Material of Water Treatment (XTCXSZ2020-3).

REFERENCES

Ayoubi-Feiz B, Aber S, Sheydaei M. Effect of oxidants on photoelectrocatalytic decolourization using α-Fe_2O_3/TiO_2/activated charcoal plate nanocomposite under visible light. RSC Adv. 2015; 5: 19368-19378.

Bouland S, Duguet J-P, Montiel A. Evaluation of bromate ions level introduced by sodium hypochlorite during post-disinfection of drinking water. Environ. Technol. 2005; 26: 121-126.

Chen F, Yang Q, Zhong Y, An H, Zhao J, Xie T, et al. Photo-reduction of bromate in drinking water by metallic Ag and reduced graphene oxide (RGO) jointly modified $BiVO_4$ under visible light irradiation. Water Res. 2016; 101: 555-563.

Cooper JK, Gul S, Toma FM, Le C, Glans PA, Guo J, et al. Electronic structure of monoclinic $BiVO_4$. Chem. Mater. 2014; 26: 5365-5373.

Gao E, Wang W, Shang M, Xu J. Synthesis and enhanced photocatalytic performance of graphene-Bi_2WO_6 composite. Phys. Chem. Chem. Phys. 2011; 13: 2887-2893.

Li R, Zhang F, Wang D, Yang J, Li M, Zhu J, et al. Spatial separation of photogenerated electrons and holes among {010} and {110} crystal facets of $BiVO_4$. Nat. Commun. 2013; 4: 1432-1439.

Li X, Pi Y, Xia Q, Li Z, Xiao J. TiO_2 encapsulated in Salicylaldehyde-NH_2-MIL-101 (Cr) for enhanced visible light-driven photodegradation of MB. Appl. Catal. B-Environ. 2016; 191: 192-201.

Li Y, Jiang Y, Ruan Z, Lin K, Yu Z, Zheng Z, et al. Simulation-guided synthesis of graphitic carbon nitride beads with 3D interconnected and continuous meso/macropore channels for enhanced light absorption and photo-catalytic performance. J. Mater. Chem. A. 2017; 5: 21300-21312.

Li Z, Dai Y, Ma X, Zhu Y, Baibiao H. Tuning photocatalytic performance of the near-infrared-driven photocatalyst $Cu_2(OH)PO_4$ based on effective mass and dipole moment. Phys. Chem. Chem. Phys. 2014; 16: 3267-3273.

Lin K-YA, Lin C-H, Chen S-Y, Yang H. Enhanced photocatalytic reduction of concentrated bromate in the presence of alcohols. Chem. Eng. J. 2016; 303: 596-603.

Liu G, Liu S, Lu Q, Sun H, Xu F, Zhao G. Synthesis of monoclinic $BiVO_4$ microribbons by sol-gel combined with electrospinning process and photocatalytic degradation performances. J. Sol-gel Sci. Techn. 2014; 70: 24-32.

Liu G, You S, Ma M, Huang H, Ren N. Removal of nitrate by photocatalytic denitrification using nonlinear optical material. Environ. Sci. Technol. 2016; 50: 11218-11225.

Liu G, You S, Tan Y, Ren N. In situ photochemical activation of sulfate for enhanced degradation of organic pollutants in water. Environ. Sci. Technol. 2017; 51: 2339-2346.

Liu G, You S, Zhang Y, Huang H, Spanjers H. Conjugated donor-acceptor (D-A) supramolecule catalyst for visible-light-driven photocatalytic removal of bromate in water. J. Colloid Interf. Sci. 2019; 553: 666-673.

Long M, Cai W, Kisch H. Visible light induced photoelectrochemical properties of n-$BiVO_4$ and n-$BiVO_4$/p-Co_3O_4. J.

Phys. Chem. C 2008; 112: 548-554.
Nakabayashi Y, Nishikawa M, Saito N, Terashima C, Fujishima A. Significance of hydroxyl radical in photoinduced oxygen evolution in water on monoclinic bismuth vanadate. J. Phys. Chem. C 2017; 121: 25624-25631.
Nie Y, Hu C, Li N, Yang L, Qu J. Inhibition of bromate formation by surface reduction in catalytic ozonation of organic pollutants over β-FeOOH/Al_2O_3. Appl. Catal. B-Environ. 2014; 147: 287-292.
Noguchi H, Nakajima A, Watanabe T, Hashimoto K. Removal of bromate ion from water using TiO_2 and alumina-loaded TiO_2 photocatalysts. Water Sci. Technol. 2002; 46: 27-31.
Noguchi H, Nakajima A, Watanabe T, Hashimoto K. Design of a photocatalyst for bromate decomposition: Surface modification of TiO_2 by pseudo-boehmite. Environ. Sci. Technol. 2003; 37: 153-157.
Pan C, Zhu Y. New type of $BiPO_4$ oxy-acid salt photocatalyst with high photocatalytic activity on degradation of dye. Environ. Sci. Technol. 2010; 44: 5570-5574.
Pan J, Liu G, Lu GQ, Cheng HM. On the true photoreactivity order of {001}, {010}, and {101} facets of anatase TiO_2 crystals. Angew. Chem. Int. Edit. 2011; 50: 2133.
Parker KM, Zeng T, Harkness J, Vengosh A, Mitch WA. Enhanced formation of disinfection byproducts in shale gas wastewater-impacted drinking water supplies. Environ. Sci. Technol. 2014; 48: 11161-9.
Perry Iv JJ, Perman JA, Zaworotko MJ. Design and synthesis of metal–organic frameworks using metal–organic polyhedra as supermolecular building blocks. Chem. Soc. Rev. 2009; 38: 1400-1417.
Romão JS, Hamdy MS, Mul G, Baltrusaitis J. Photocatalytic decomposition of cortisone acetate in aqueous solution. J. Hazard. Mater. 2015; 282: 208-215.
Saison T, Chemin N, Chanéac C, Durupthy O, Mariey L, Maugé Fo, et al. New insights into $BiVO_4$ properties as visible light photocatalyst. J. Phys. Chem. C 2015; 119: 12967-12977.
Shen W, Lin F, Jiang X, Li H, Ai Z, Zhang L. Efficient removal of bromate with core-shell Fe@Fe_2O_3 nanowires. Chem. Eng. J. 2017; 308: 880-888.
Stoltzfus MW, Woodward PM, Ram S, Jae-Hyun K, Bruce B. Structure and bonding in $SnWO_4$, $PbWO_4$, and $BiVO_4$: lone pairs vs inert pairs. Inorg. Chem. 2007; 46: 3839-50.
Su J, Guo L, Bao N, Grimes CA. Nanostructured WO_3/$BiVO_4$ Heterojunction films for efficient photoelectrochemical water splitting. Nano Lett. 2011; 11: 1928-1933.
Wang D, Jiang H, Zong X, Xu Q, Ma Y, Li G, et al. Crystal facet dependence of water oxidation on $BiVO_4$ sheets under visible light irradiation. Chem. Eur. J. 2011; 17: 1275-1282.
Wang Q, Snyder S, Kim J, Choi H. Aqueous ethanol modified nanoscale zerovalent iron in bromate reduction: synthesis, characterization, and reactivity. Environ. Sci. Technol. 2009; 43: 3292-3299.
Wang W, Han Q, Zhu Z, Zhang L, Zhong S, Liu B. Enhanced photocatalytic degradation performance of organic contaminants by heterojunction photocatalyst $BiVO_4$/TiO_2/RGO and its compatibility on four different tetracycline antibiotics. Adv. Powder Technol. 2019; 30: 1882-1896.
Wang Y, Ding K, Xu R, Yu D, Wang W, Gao P, et al. Fabrication of $BiVO_4$/$BiPO_4$/GO composite photocatalytic material for the visible light-driven degradation. J. Clean. Prod. 2020a; 247: 119108.
Wang Y, Yu D, Wang W, Gao P, Zhong S, Zhang L, et al. Synthesizing Co_3O_4-$BiVO_4$/g-C_3N_4 heterojunction composites for superior photocatalytic redox activity. Sep. Purif. Technol. 2020b; 239: 116562.
Weinberg HS, Delcomyn CA, Unnam V. Bromate in chlorinated drinking waters: occurrence and implications for future regulation. Environ. Sci. Technol. 2003; 37: 3104-3110.
Williams G, Seger B, Kamat PV. TiO_2-graphene nanocomposites. UV-assisted photocatalytic reduction of graphene oxide. ACS Nano 2008; 2: 1487-1491.
Wu X, Yang Q, Xu D, Zhong Y, Luo K, Li X, et al. Simultaneous adsorption/reduction of bromate by nanoscale zerovalent iron supported on modified activated carbon. Ind. Eng. Chem. Res. 2013; 52: 12574-12581.

Xie L, Shang C. The effects of operational parameters and common anions on the reactivity of zero-valent iron in bromate reduction. Chemosphere 2007; 66: 1652-1659.

Xu Y, Schoonen MAA. The absolute Energy position of conduction and valence bands of selected semiconducting minerals. Am. Mineral. 2000; 85: 543-556.

Yang J, Wang D, Zhou X, Li C. A theoretical study on the mechanism of photocatalytic oxygen evolution on $BiVO_4$ in aqueous solution. Chem. Eur. J. 2013; 19: 1320-1326.

Yang R, Dong F, You X, Liu M, Zhong S, Zhang L, et al. Facile synthesis and characterization of interface charge transfer heterojunction of Bi_2MoO_6 modified by Ag/AgCl photosensitive material with enhanced photocatalytic activity. Mater. Lett. 2019; 252: 272-276.

Yang R, Zhong S, Zhang L, Liu B. PW12/CN@ Bi_2WO_6 composite photocatalyst prepared based on organic-inorganic hybrid system for removing pollutants in water. Sep. Purif. Technol. 2020a; 235: 116270.

Yang R, Zhu Z, Hu C, Zhong S, Zhang L, Liu B, et al. One-step preparation (3D/2D/2D) $BiVO_4$/$FeVO_4$@rGO heterojunction composite photocatalyst for the removal of tetracycline and hexavalent chromium ions in water. Chem. Eng. J. 2020b; 390: 124522.

Zhang F, Jin R, Chen J, Shao C, Gao W, Li L, et al. High photocatalytic activity and selectivity for nitrogen in nitrate reduction on Ag/TiO_2 catalyst with fine silver clusters. J. Catal. 2005; 232: 424-431.

Zhang H, Yu D, Wang W, Gao P, Zhang L, Zhong S, et al. Construction of a novel BON-Br-AgBr heterojunction photocatalysts as a direct Z-scheme system for efficient visible photocatalytic activity. Appl. Surf. Sci. 2019; 497: 143820.

Zhang Y, Jing S, Liu H. Reactivity and mechanism of bromate reduction from aqueous solution using Zn–Fe(II)–Al layered double hydroxides. Chem. Eng. J. 2015; 266: 21-27.

Zhu J, Pang S, Dittrich T, Gao Y, Nie W, Cui J, et al. Visualizing the nano cocatalyst aligned electric fields on single photocatalyst particles. Nano Lett. 2017; 17: 6735-6741.

Zhu Y, Li J, Dong C, Ren J, Huang Y, Zhao D, et al. Red phosphorus decorated and doped TiO_2 nanofibers for efficient photocatalytic hydrogen evolution from pure water. Appl. Catal. B-Environ. 2019; 255: 117764.

Zhu Y, Lv C, Yin Z, Ren J, Yang D. A [001]- Oriented hittorf's phosphorus nanorods/polymeric carbon nitride heterostructure for boosting wide- spectrum- responsive photocatalytic hydrogen evolution from pure water. Angew. Chem. Int. Edi. 2020a; 59: 868-873.

Zhu Y, Ren J, Zhang X, Yang D. Elemental red phosphorus-based materials for photocatalytic water purification and hydrogen production. Nanoscale 2020b, 12, 13297-13310

Zhu Z, Wang C, Liang L, Yu D, Sun J, Zhang L, et al. Synthesis of novel ternary photocatalyst Ag_3PO_4/Bi_2WO_6/multi-walled carbon nanotubes and its enhanced visible-light photoactivity for photodegradation of norfloxacin. J. Nanosci. Nano. 2020c; 20: 2247-2258.

Table List

Table 1 Summary of the effective masses

	{010}/m_0	{110}/m_0
m_h^*	0.18	0.57
m_e^*	0.13	0.30

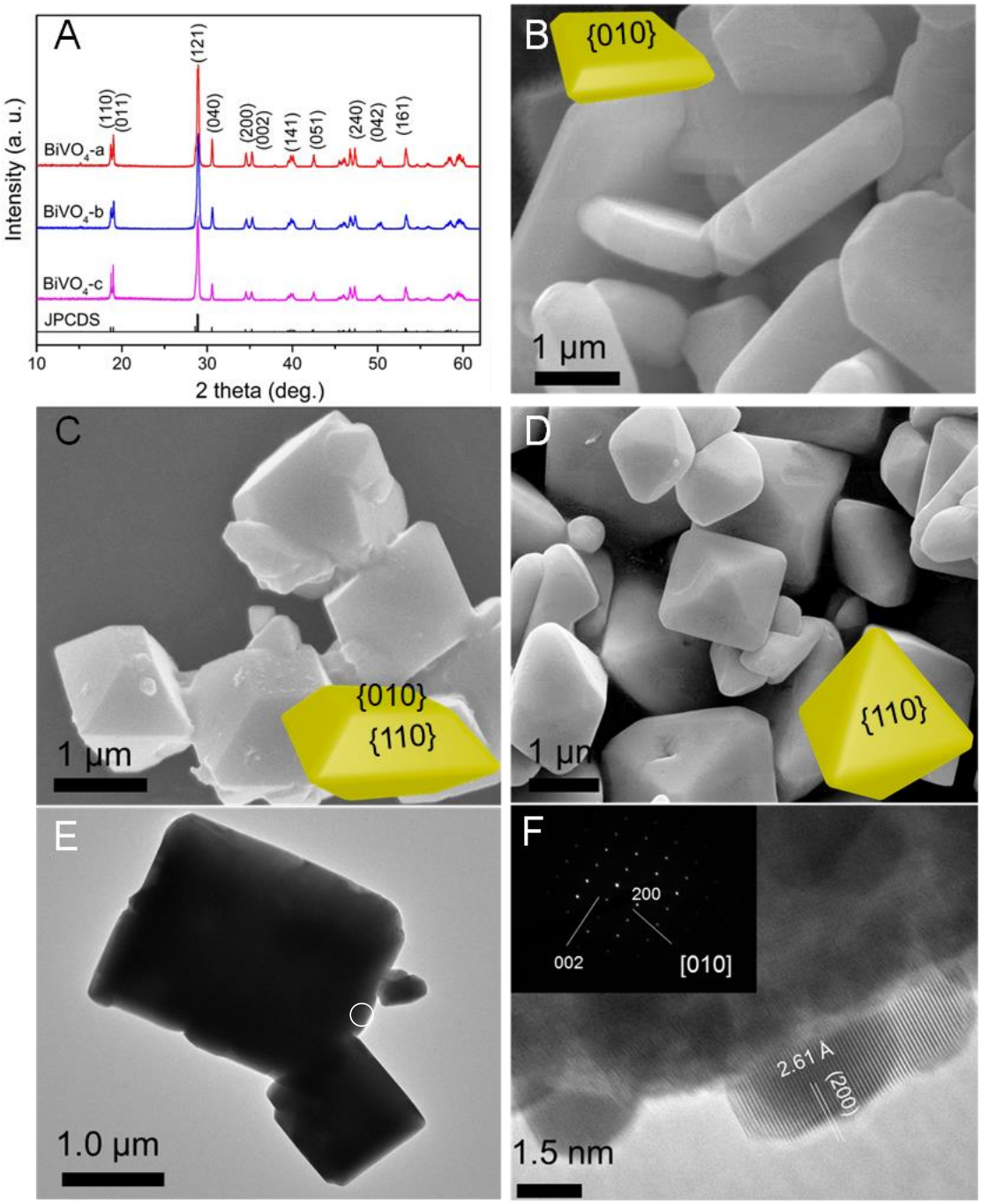

Figure 1 XRD patterns of (A) $BiVO_4$ samples, SEM pictures of (B) $BiVO_4$-a, (C) $BiVO_4$-b, (D) $BiVO_4$-c, (E) TEM and HRTEM (F) pictures of $BiVO_4$-a.

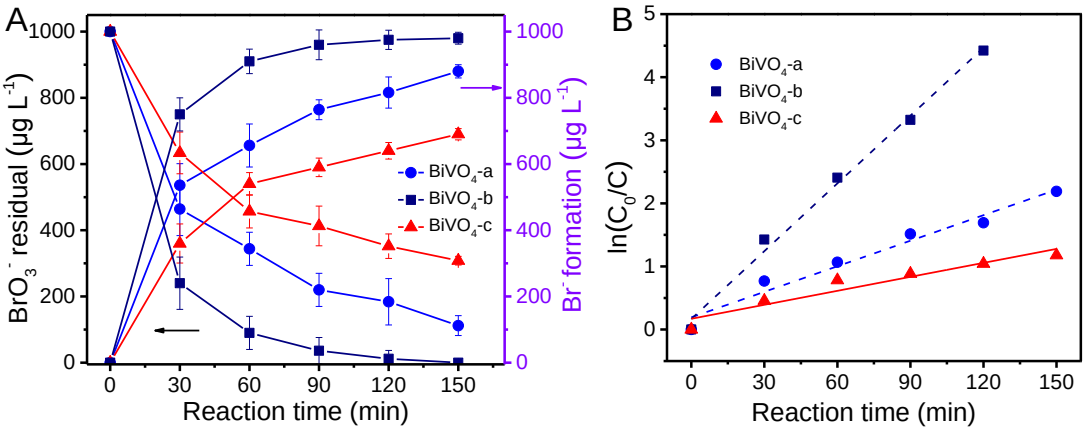

Figure 2 Time course of (A) photocatalytic reduction of BrO_3^- by $BiVO_4$ photocatalysts under visible light irradiation at pH 7.1±0.4, (B) the corresponding kinetics rate constants derived from A.

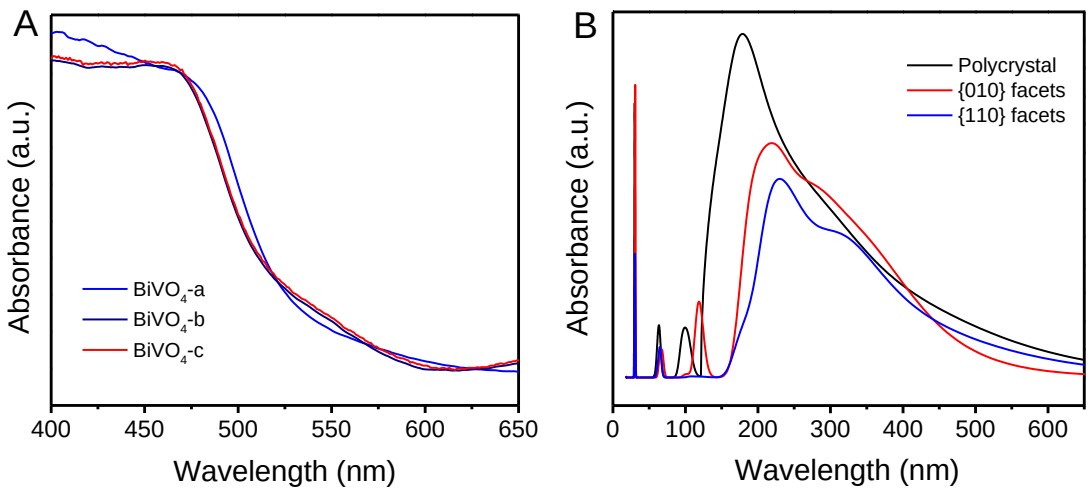

Figure 3 (A) The experimental diffuse reflectance spectra of $BiVO_4$ samples, (B) calculated absorption coefficient of polycrstal $BiVO_4$, {010} and {110} facets exposed $BiVO_4$.

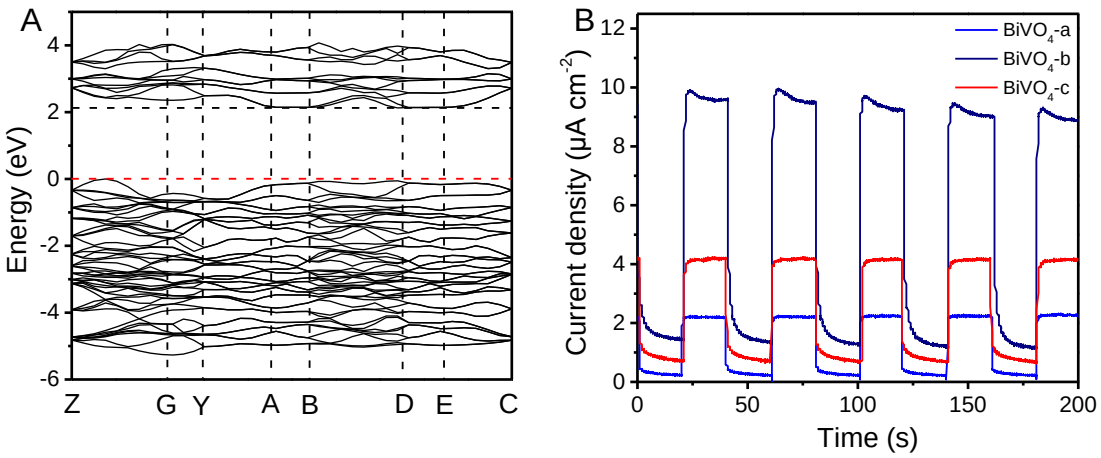

Figure 4 The band structure (A) of $BiVO_4$ crystal and (B) photocurrent-time curve of $BiVO_4$ samples.

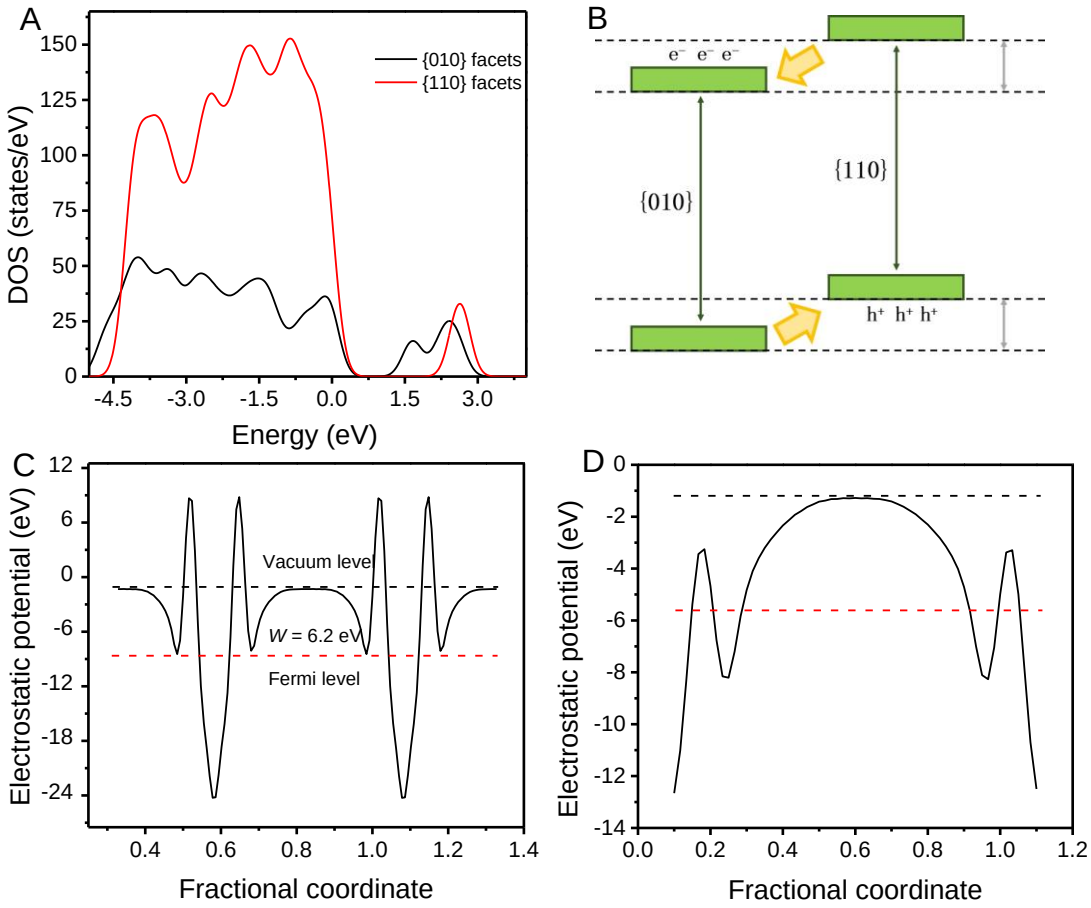

Figure 5 (A) The differences of the energy levels in conduction bands (Δ_{CB}) for {010} and {110} facets, (B) the scheme of carrier separation between {010} and {110} facets, (C) the workfunction (W) of {010} surface and (D) {110} surface.

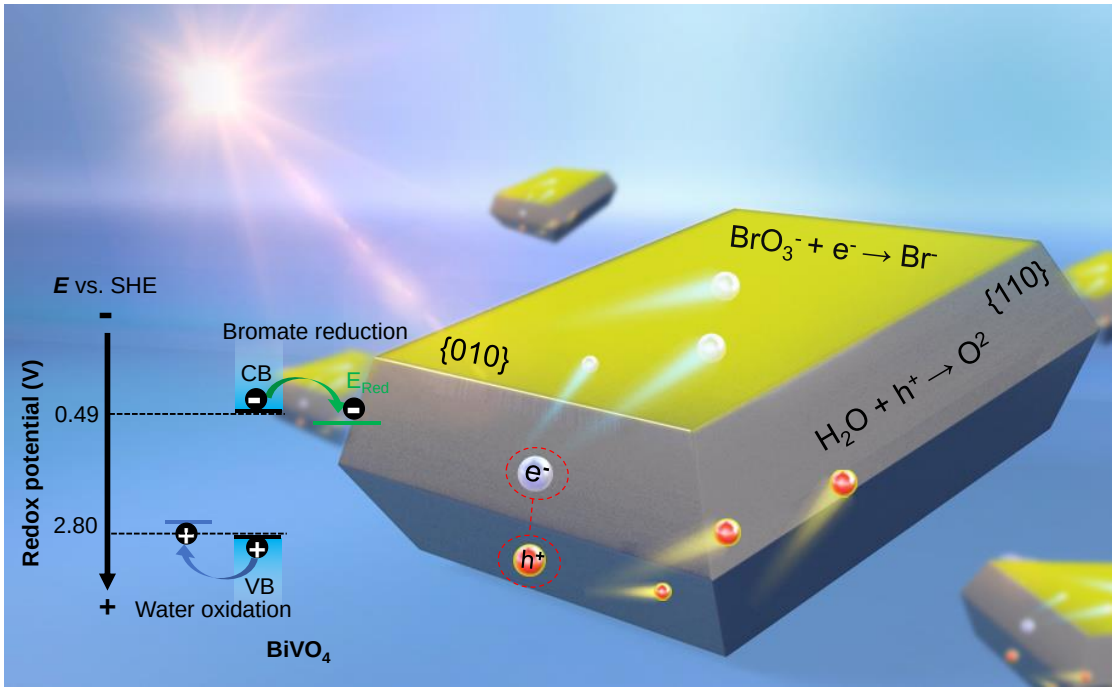

Figure 6 Schematic illustration of photocatalytic reduction of BrO_3^- by $BiVO_4$-b.